



Short communication

Unusual ageing behaviour of friction-stir welded Al–Cu–Mg alloy

Ivan S. Zuiko^{*}, Sergey Mironov, Rustam Kaibyshev

Belgorod National Research University, Pobeda 85, Belgorod, 308015, Russia



ARTICLE INFO

Keywords:

Heat-treatable aluminium alloys
Friction-stir welding
Microstructure
Second-phase particles
Microstructure-strength relationship

ABSTRACT

The conventional peak-ageing treatment of friction-stir welded AA2519 resulted in precipitation of a stable θ -phase instead of the expected strengthening dispersoids of θ'' and θ' thus degrading material strength. This phenomenon was attributed to acceleration of the precipitation kinetics due to grain refinement and over-ageing effect associated with the weld thermal cycle.

1. Introduction

Friction-stir welding (FSW) is an innovative technology that enables a successful joining of a wide range of metallic materials including even those which are conventionally believed to be «unweldable» [1]. In heat-treatable aluminum alloys, however, a joint efficiency of friction-stir welds is typically low [2]. This effect is usually attributed to the complex precipitation phenomena occurring during welding of such materials. Specifically, at relatively low welding temperatures, a considerable coarsening of strengthening agents is usually found [e.g. Ref. [3–11]]. This normally results in the coherency loss between the precipitates and aluminum matrix [e.g. Ref. [5,8]]. At relatively high temperatures, the second-phase particles may dissolve [e.g. Ref. [3–9, 12]]. All above processes give rise to material softening and thus essentially degrade weld strength [e.g. Refs. [6,8]]. Importantly, due to the significant temperature gradient inherent to FSW, they occur simultaneously, in different locations, or so-called “microstructural zones”, of the weld, thus giving rise to a pronounced microstructural heterogeneity. As a result, the weld strength cannot be recovered by using the standard post-weld ageing procedure, since it enhances the over-ageing effect in the heat-affected zone. Instead, an application of a T6 re-treatment (i.e., solutionizing treatment followed by artificial ageing) is required. However, the solution treatment of the friction-stirred materials often results in the abnormal grain growth [e.g. Ref. [13–15]], which is also an undesirable effect. Considering the importance of the heat-treatable aluminum alloys for industry, significant efforts have been undertaken recently to overcome the above difficulties but no appropriate solution has been found up to now.

In this work, a new approach was suggested for this purpose. To avoid the undesirable effects associated with the coagulation and/or dissolution of secondary phase, it was proposed to weld these alloys in the particle-free material condition. It was suggested that the subsequent ageing of the produced welds could provide a uniform distribution of the strengthening nano-scale precipitates and thus results in a nearly-100 pct. joint efficiency. Despite the aforementioned idea is quite trivial, it has not been reported in the scientific literature so far, to the best of the authors' knowledge. Therefore, the present study aimed to examine the reliability of this approach.

2. Experimental

The material used in the present work was a commercial aluminum alloy 2519 with a nominal chemical composition of Al–5.64Cu–0.33Mn–0.23Mg–0.15Zr–0.11Ti–0.09V–0.08Fe–0.08Zn–0.04Sn–0.01Si (all in wt. pct.). This is a typical heat-treatable alloy whose precipitation path is studied relatively well [16–19]. The material was produced by ingot casting, homogenized at 510 °C for 24 h and then recrystallized by rolling at 425 °C to a true strain of 0.88. In order to produce the T820 temper condition, the hot-rolled material was solutionized at 535 °C for 1 h, water quenched and then cold rolled to a true thickness reduction of 0.22¹. Prior to the subsequent artificial ageing, the cold-rolled material was friction-stir welded, in accordance with the idea described in the **Introduction** section. To examine a possible influence of the weld heat input, two different FSW regimes were used, as shown in **Table 1**. In all cases, the welding tool was fabricated from a tool steel and consisted of a shoulder of 12.5 mm in diameter and an M5

^{*} Corresponding author.,

E-mail addresses: zuiko_ivan@bsu.edu.ru, zuiko.ivan@gmail.com (I.S. Zuiko).

¹ Typical microstructure of the cold-rolled material is shown in **Supplementary Fig. S1**.

Table 1
FSW conditions used in this work.

Spindle rate, rpm	Feed rate, mm/min	Weld designation
500	760	Low heat-input weld
1100	380	High heat-input weld

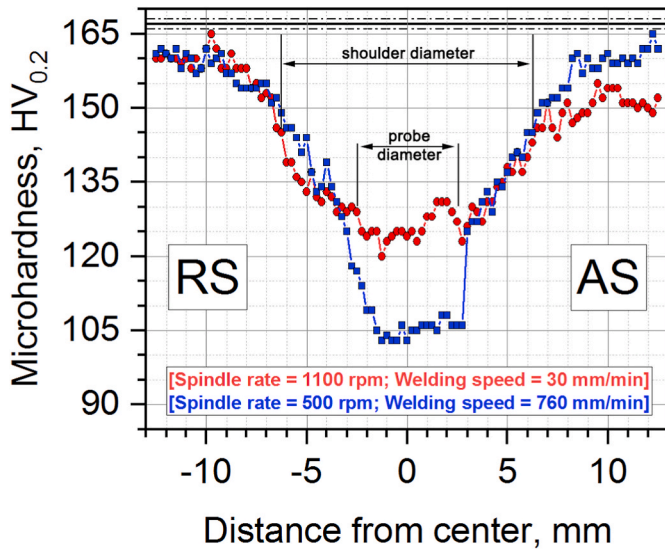


Fig. 1. Microhardness profiles measured across transverse cross-sections of the low- and high-heat-input welds. RS and AS denote retreating side and advancing side, respectively. The solid horizontal line show the mean microhardness measured far away from the weld zone (the dotted lines delineate the standard deviation of the measurements). Note: Both welds were subjected to the peak-ageing treatment prior to the microhardness measurements.

cylindrical probe of 2.7 mm in length. Following FSW, the produced joints were aged at 165 °C for 6 h. The ageing durations were selected on the basis of the preliminary experiments illustrated in [Supplementary Figs. S2 and S3](#).

To evaluate the precipitation behaviour of the produced joints, microhardness profiles were measured and the microstructures were studied with transmission electron microscopy (TEM). The Vickers microhardness was measured across the weld mid-thickness by applying a load of 200 g with a dwell time of 10 s. The microstructural observations were conducted with a JEM-2100 TEM operating at 200 kV. Foils were cut directly from the center of welds (i.e. from the nugget region) and prepared in a standard way. Additional experimental details could be found in Refs. [16–18].

It should be stressed that all microstructural observations and microhardness measurements in this work were conducted on the post-weld aged samples.

3. Results and discussion

3.1. Weld strength

Microhardness profiles measured across transverse cross-section of the aged joints are presented in [Fig. 1](#). A significant material softening is evident in the weld zone with the effect being most pronounced for the low heat-input weld. This means that the initial idea of this work was erroneous.

Since the material was welded in the particle-free condition, it may be suggested that the revealed softening effect (i.e. drop in microhardness) was associated with a difference in the post-weld ageing behaviour between base and welded material. To check this assumption, these two microstructural regions were investigated by TEM.

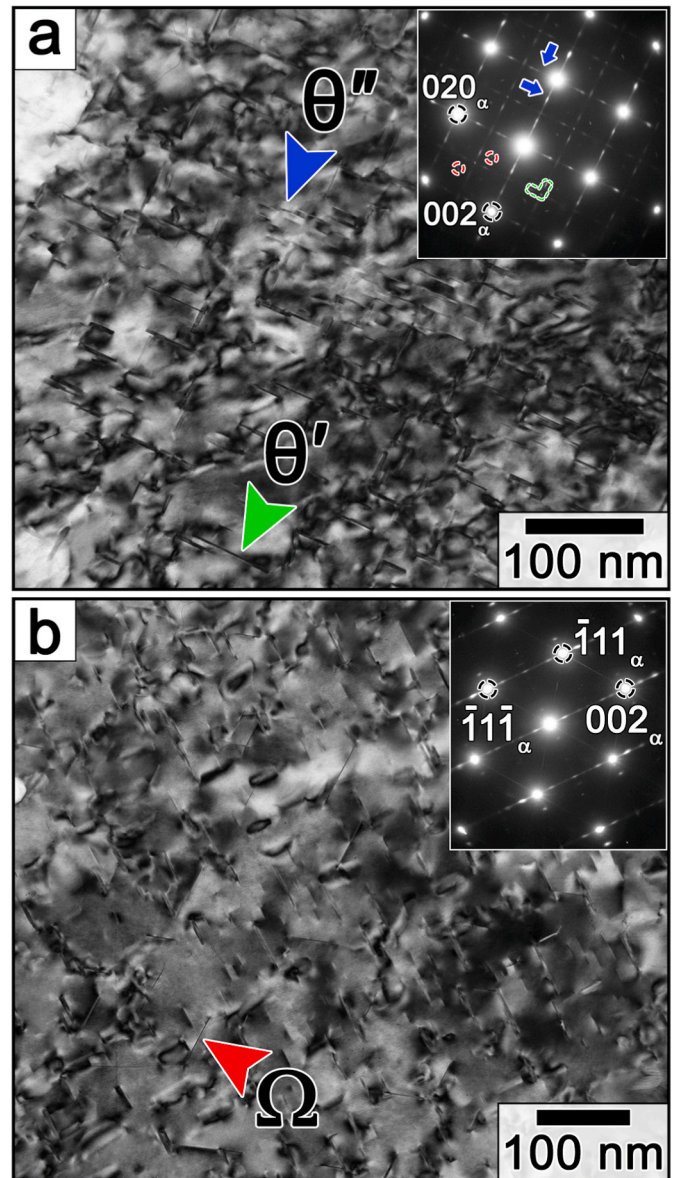


Fig. 2. TEM-micrographs and corresponding SAED patterns (insets) taken from the base material zone. In (a), the material is shown in the near- $\langle 001 \rangle$ orientation to emphasize the constituent θ' and θ'' phases (exemplified by the green and blue arrows, respectively). In (b), the material is shown in the near- $\langle 110 \rangle$ orientation to emphasize the Ω phase (exemplified by the red arrow). In the diffraction pattern in (a), the reflections from the θ' -, θ'' - and Ω -phases are exemplified by green arrow, blue arrows and red circles, respectively (in greater details, the interpretation of the diffraction pattern is described in Ref. [16–18]). (For interpretation of the references to colour in this figure legend, the reader is referred to the Web version of this article.)

3.2. Microstructure in the base material zone

In the base material zone, as expected, a precipitation of the coherent θ'' and semi-coherent θ' -, as well as Ω -phases was revealed ([Fig. 2](#)). Specifically, an alignment of two variants (from three possible) of the θ'/θ'' phases along orthogonal $\{001\}_\alpha$ planes is seen in [Fig. 2a](#). Moreover, the selected-area diffraction (SAED) pattern taken from this area additionally exhibited the intensity maxima at $1/3$ and $2/3$ $[220]_\alpha$ (red circles in the insert in [Fig. 2a](#)) attributable to the Ω -phase [16–19]. The TEM micrograph taken from the $\langle 011 \rangle_\alpha$ direction ([Fig. 2b](#)) as well as the streaking along the $\langle 111 \rangle_\alpha$ in SAED pattern (inset in [Fig. 2b](#)) are evidence of the precipitation of the plate-shaped Ω particles habiting on

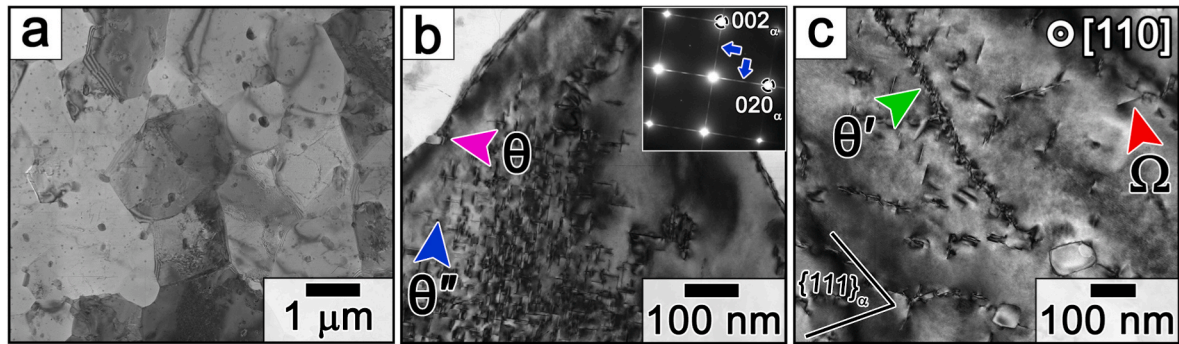


Fig. 3. TEM micrographs showing the typical grain structure (a) and the characteristic precipitation patterns (b, c) observed in the low-heat-input weld. In (b), the material is shown in the near- $\langle 001 \rangle_{\alpha}$ orientation to emphasize the θ'' -phase (exemplified by the blue arrow). In (c), the material is shown in the near- $\langle 011 \rangle_{\alpha}$ orientation to emphasize the Ω phase (exemplified by the red arrow). In (b), the insert at the upper right corner shows a characteristic micro-diffraction pattern with the discontinuous streaks (exemplified by blue arrows) associated with the θ'' -phase. Note: The welded material was subjected to the peak-ageing treatment prior to the microstructural observations. See text for details. (For interpretation of the references to colour in this figure legend, the reader is referred to the Web version of this article.)

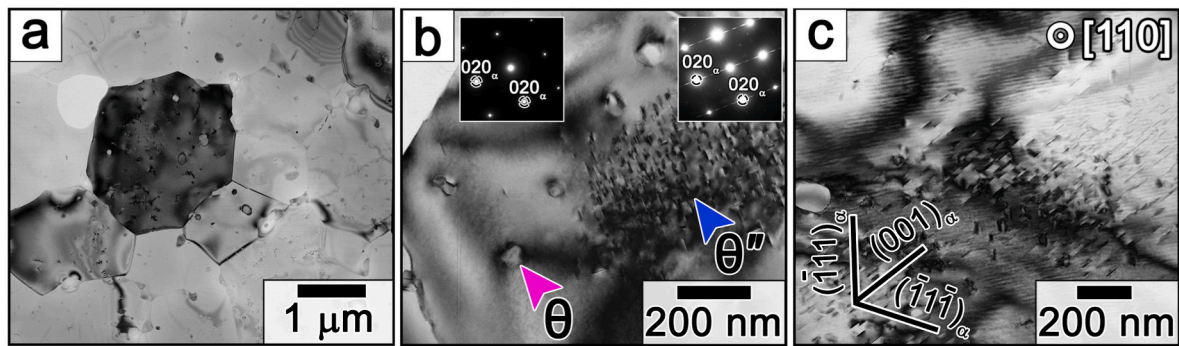


Fig. 4. TEM-images showing the typical grain structure (a) and the characteristic precipitation patterns (b, c) observed in the high-heat-input weld. In (b), the material is shown in the near- $\langle 001 \rangle_{\alpha}$ orientation to emphasize the θ'' -phase (exemplified by the blue arrow). In (b), the inserts in the upper section show the micro-diffraction patterns taken from aluminum matrix (left), and from the local area enriched by the θ'' -phase (right). Note: The welded material was subjected to the peak-ageing treatment prior to the microstructural observations. See text for details. (For interpretation of the references to colour in this figure legend, the reader is referred to the Web version of this article.)

the $\{111\}_{\alpha}$ planes. A nearly uniform distribution of the above strengthening agents within the grain interior (Fig. 2) expectedly resulted in a relatively high strength of the base material zone (Fig. 1, S2 and S3).

3.3. Microstructure in the stir zone

The characteristic TEM-micrographs taken from the stir zone of the low- and the high heat-input welds are given in Figs. 3 and 4, respectively. In both cases, the developed microstructures were dominated by relatively fine equiaxed grains containing low dislocation density (Figs. 3a and 4a). Such structures are normally observed in friction-stirred aluminum alloys and are usually ascribed to the dynamic recrystallization occurring during FSW [1,2]. Thus, the fine-grained recrystallized microstructure evolved in the stir zone was distinctly different from the coarse-grained, heavily deformed base material [18]. This leads to essentially different precipitation behaviour during subsequent ageing treatment.

First and foremost, a phase composition of the aged stir zone is markedly different from that of the aged base material. Specifically, the volume fraction of nano-scale θ' , θ'' and Ω particles apparently decreased (cf. Fig. 3b-c, 4b-c and 2). On the other hand, a precipitation of relatively coarse, incoherent θ -phase was found (pink arrows in Figs. 3b and 4b and Supplementary Fig. S4). Traditionally θ nucleates at interphase θ' /matrix interfaces, grain boundaries or directly from matrix if ageing temperature is high enough [19]. Second, it is obvious that the particle

distribution was highly inhomogeneous. Particularly, the precipitates were often found to nucleate at grain boundaries (pink arrow in Fig. 3b) or sub-grain boundaries (green arrow in Fig. 3c). It is surprising that the distribution of the coherent θ'' -phase in the grain interior was also non-uniform (Figs. 3b and 4b).

It seems therefore that the considerable material softening observed in the weld zone (Fig. 1) was associated with heterogeneous nucleation and substantial coarsening of the strengthening precipitates.

3.4. Ageing behaviour of the stir zone material

It is relatively well accepted that precipitation of the secondary phases in Al-Cu-Mg alloys (with Cu/Mg ratio >5.6) usually goes through the following sequences of the transformation steps [19]:

- (1) SSSS \rightarrow $\{001\}$ clusters \rightarrow GP zones \rightarrow θ'' -phase \rightarrow θ' -phase \rightarrow θ -phase;
- (2) SSSS \rightarrow $\{111\}$ clusters \rightarrow Ω -phase \rightarrow θ -phase,

where SSSS stands for supersaturated solid solution and GP stands for Guinier-Preston zones. The (1) and (2) reactions take place on $\{100\}_{\alpha}$ and $\{111\}_{\alpha}$, respectively.

In this context, the nucleation of the stable θ -phase at the expense of the transition θ'' -, θ' - and Ω -phases observed in the stir zone in the present study virtually implies a considerable acceleration of the phase transformations.

An obvious reason for this effect is the significant grain refinement

occurred in the stir zone. The enhanced diffusion along the grain- and sub-grain boundaries should give rise to the heterogeneous nucleation of the second-phase particles and promote their rapid further evolution. Another possibility may be a relatively high concentration of vacancies in the stir zone due to the very large high-temperature deformation imposed during FSW [1,2].

It should be also added that the unusual particle behaviour of the stir zone material may be associated with the FSW thermal cycle. It is important to emphasize that the peak FSW temperature in aluminum alloys may vary from ~ 150 °C to ~ 480 °C [20], whereas the θ''/θ' phases in the studied alloy usually precipitate above ~ 100 °C [17,19] and the θ -phase dissolves in the temperature range of 270–540 °C (Supplementary Fig. S5). This means that FSW could have caused the precipitation of a secondary phase, and a fraction of it may have been present in the stirred material. During post-weld ageing, these particles may coarsen thus causing material softening. This effect should be most pronounced in the low-heat-input weld (Fig. 3), because the FSW temperature in this case may be high enough for the particle precipitation but low for their subsequent dissolution. This agrees well with microhardness measurements shown in Fig. 1.

Therefore, due to the drastic changes in the grain structure induced by FSW as well as the partial precipitation of the secondary particles occurring during weld thermal cycle, the ageing behaviour of the stir zone material should be essentially different from that of the base material. Based on this philosophy, it seems that the conception proposed in the Introduction section of this manuscript was fundamentally erroneous.

4. Conclusion

The drastic microstructural changes induced by FSW exerted a significant influence on the following ageing behaviour of the stir zone material. Specifically, the grain refinement provides heterogeneous nucleation of the secondary particles and essentially accelerates the phase transformation rate. As a consequence, a relatively coarse and incoherent particles develop near grain boundaries instead of the expected nano-scale homogeneously distributed strengthening agents in grain interior. Moreover, the FSW thermal cycle inevitably leads to the precipitation of the second-phase particles and considerable portion of which may retain in the final stir zone material. Hence, the standard post-weld ageing results in the over-ageing effect and the concomitant material softening.

Originality statement

I write on behalf of myself and all co-authors to confirm that the results reported in the manuscript are original and neither the entire work, nor any of its parts have been previously published. The authors confirm that the article has not been submitted to peer review, nor has been accepted for publishing in another journal. The author(s) confirms that the research in their work is original, and that all the data given in the article are real and authentic. If necessary, the article can be recalled, and errors corrected.

Data availability

All data included to this study are available upon request by contact with corresponding author.

Declaration of competing interest

The authors declare that they have no known competing financial interests or personal relationships that could have appeared to influence the work reported in this paper.

CRedit authorship contribution statement

Ivan S. Zuiko: Methodology, Investigation, Formal analysis, Writing - original draft, Visualization. **Sergey Mironov:** Conceptualization, Methodology, Writing - review & editing, Supervision. **Rustam Kaibyshev:** Conceptualization, Resources, Funding acquisition.

Acknowledgments

This work was financially supported by the Russian Science Foundation under Grant N \circ 19-79-00304. The authors are grateful to the personnel of the Joint Research Center “Technology and Materials” at Belgorod National Research University and to Dr. S. Malopheyev for experimental assistance.

Appendix A. Supplementary data

Supplementary data to this article can be found online at <https://doi.org/10.1016/j.msea.2020.139882>.

References

- [1] R.S. Mishra, Z.Y. Ma, Friction stir welding and processing, *Mater. Sci. Eng. R* 50 (2005) 1–78, <https://doi.org/10.1016/j.mser.2005.07.001>.
- [2] P.L. Threadgill, A.J. Leonard, H.R. Shercliff, P.J. Withers, Friction stir welding of aluminum alloys, *Int. Mater. Rev.* 54 (2009) 49–93, <https://doi.org/10.1179/174328009X411136>.
- [3] J.-Q. Su, T.W. Nelson, R. Mishra, M. Mahoney, Microstructural investigation of friction stir welded 7050-T651 aluminum, *Acta Mater.* 51 (2003) 713–729, [https://doi.org/10.1016/s1359-6454\(02\)00449-4](https://doi.org/10.1016/s1359-6454(02)00449-4).
- [4] M. Dumont, A. Steuwer, A. Deschamps, M. Peel, P.J. Withers, Microstructure mapping in friction stir welds of 7449 aluminum alloy using SAXS, *Acta Mater.* 54 (2006) 4793–4801, <https://doi.org/10.1016/j.actamat.2006.06.015>.
- [5] A. Sumar, Y. Brechet, B. de Meester, A. Denquin, T. Pardoën, Microstructure, local and global mechanical properties of friction stir welds in aluminum alloy 6005A-T6, *Mater. Sci. Eng.* 486 (2008) 85–95, <https://doi.org/10.1016/j.msea.2007.08.041>.
- [6] C. Genevois, A. Deschamps, A. Denquin, B. Doisneau-Cottignies, Quantitative investigation of precipitation and mechanical behavior for AA2024 friction stir welds, *Acta Mater.* 53 (2005) 2447–2458, <https://doi.org/10.1016/j.actamat.2005.02.007>.
- [7] M.J. Jones, P. Heurtier, C. Desrayaud, F. Montheillet, D. Allehaux, J.H. Driver, Correlation between microstructure and microhardness in a friction stir welded 2024 aluminum alloy, *Scripta Mater.* 52 (2005) 693–697, <https://doi.org/10.1016/j.scriptamat.2004.12.027>.
- [8] R.W. Fonda, J.F. Bingert, Microstructural evolution in the heat-affected zone of a friction stir weld, *Metall. Mater. Trans.* 35 (2004) 1487–1499, <https://doi.org/10.1007/s11661-004-0257-7>.
- [9] A. Steuwer, M. Dumont, J. Altenkirch, S. Biroasca, A. Deschamps, P.B. Prangnell, P. J. Withers, A combined approach to microstructure mapping of an Al-Li AA2199 friction stir weld, *Acta Mater.* 59 (2011) 3002–3011, <https://doi.org/10.1016/j.actamat.2011.01.040>.
- [10] A. Simar, Y. Brechet, B. de Meester, A. Denquin, T. Pardoën, Sequential modeling of local precipitation, strength and strain hardening in friction stir welds of an aluminum alloy 6005A-T6, *Acta Mater.* 55 (2007) 6133–6143, [10.1016/j.actamat.2007.07.012](https://doi.org/10.1016/j.actamat.2007.07.012).
- [11] N. Kamp, A. Sullivan, R. Tomas, J.D. Robson, Modelling of heterogeneous precipitate distribution evolution during friction stir welding process, *Acta Mater.* 54 (2006) 2003–2014, <https://doi.org/10.1016/j.actamat.2005.12.024>.
- [12] C.G. Rhodes, M.W. Mahoney, W.H. Bingel, R.A. Spurling, C.C. Bampton, Effects of friction stir welding on microstructure of 7075 aluminum, *Scripta Mater.* 36 (1997) 69–75, [https://doi.org/10.1016/S1359-6462\(96\)00344-2](https://doi.org/10.1016/S1359-6462(96)00344-2).
- [13] I. Charit, R.S. Mishra, Abnormal grain growth in friction stir processed alloys, *Scripta Mater.* 58 (2008) 367–371, <https://doi.org/10.1016/j.scriptamat.2007.09.052>.
- [14] Kh.A.A. Hassan, A.F. Norman, D.A. Price, P.B. Prangnell, Stability of nugget zone grain structures in high strength Al-alloy friction stir welds during solution treatment, *Acta Mater.* 51 (2003) 1923–1936, [https://doi.org/10.1016/S1359-6454\(02\)00598-0](https://doi.org/10.1016/S1359-6454(02)00598-0).
- [15] S. Mironov, K. Masaki, Y.S. Sato, H. Kokawa, Relationship between material flow and abnormal grain growth in friction-stir welds, *Scripta Mater.* 67 (2012) 983–986, <https://doi.org/10.1016/j.scriptamat.2012.09.002>.
- [16] I. Zuiko, R. Kaibyshev, Effect of plastic deformation on the aging behaviour of an Al–Cu–Mg alloy with a high Cu/Mg ratio, *Mater. Sci. Eng. A* 737 (2018) 401–412, <https://doi.org/10.1016/j.msea.2018.09.017>.
- [17] I. Zuiko, R. Kaibyshev, Aging behavior of an Al–Cu–Mg alloy, *J. Alloys Compd.* 759 (2018) 108–119, <https://doi.org/10.1016/j.jallcom.2018.05.053>.

- [18] I.S. Zuiiko, R. Kaibyshev, Ageing response of cold-rolled Al–Cu–Mg alloy, *Mater. Sci. Eng. A* 781 (2020) 139148, <https://doi.org/10.1016/j.msea.2020.139148>.
- [19] S.C. Wang, M.J. Starink, Precipitates and intermetallic phases in precipitation hardening Al–Cu–Mg–(Li) based alloys, *Int. Mater. Rev.* 50 (2005) 193–215, <https://doi.org/10.1179/174328005X14357>.
- [20] S. Mironov, K. Inagaki, Y.S. Sato, H. Kokawa, Effect of welding temperature on microstructure of friction-stir welded aluminum alloy 10509, *Metall. Mater. Trans.* 46 (2015) 783–790, <https://doi.org/10.1007/s11661-014-2651-0>.